Original Article

MOLECULAR METABOLISM

Effects of children's microbiota on adipose and intestinal development in sex-matched mice persist into adulthood following a single fecal microbiota transplantation

Federica La Rosa[1,7], Maria Angela Guzzardi[1,*,7], Mercedes Pardo-Tendero[2], Monica Barone[3], Chiara Ruocco[4], Gabriele Conti[3], Daniele Panetta[1], Daria Riabitch[1], Silvia Bernardi[1], Assuero Giorgetti[5], Daniela Campani[6], Daniel Monleon[2], Enzo Nisoli[4], Patrizia Brigidi[3], Patricia Iozzo[1,]**

ABSTRACT

Background: The global prevalence of obesity and type 2 diabetes, particularly among children, is rising, yet the long-term impacts of early-life fecal microbiota transplantation (FMT) on metabolic health remain poorly understood.
Objectives: To investigate how early-life FMT from children to young, sex-matched mice influences metabolic outcomes and adipose tissue function in later, adult life.
Methods: Germ-free mice were colonized with fecal microbiota from either lean children or children with obesity. The impacts on brown adipose tissue (BAT), white adipose tissue (WAT), glucose metabolism, and gut health were analyzed in male and female mice. Microbial communities and metabolite profiles were characterized using sequencing and metabolomics.
Results: Male mice receiving FMT from obese donors exhibited marked BAT whitening and impaired amino acid and glucose metabolism. In contrast, female recipients developed hyperglycemia, accompanied by gut barrier dysfunction and WAT impairment. Distinct microbial and metabolite profiles were associated with these phenotypes: *Collinsella* and trimethylamine in females; and *Paraprevotella*, *Collinsella*, *Lachnospiraceae NK4A136*, *Bacteroides*, *Coprobacillus*, and multiple metabolites in males. These phenotypic effects persisted despite changes in host environment and diet.
Conclusions: Early-life FMT induced long-lasting effects on the metabolic landscape, profoundly affecting adipose tissue function and systemic glucose homeostasis in adulthood. Donor dietary habits correlated with the fecal microbial profiles observed in recipient mice. These findings highlight the critical need for identifying and leveraging beneficial exposures during early development to combat obesity and diabetes.

Keywords Obesity; Type 2 diabetes; Positron emission tomography; Gut microbiota; Metabolomics; Adipose tissue; Intestinal permeability

[1]Institute of Clinical Physiology, National Research Council, via Moruzzi 1, 56124 Pisa, Italy [2]Department of Pathology, University of Valencia, Health Research Institute INCLIVA/CIBERFES for Frailty and Healthy Aging, Blasco Ibañez, 15, 46010, Valencia, Spain [3]Human Microbiomics Unit, Department of Medical and Surgical Sciences, University of Bologna, via Massarenti 9, 40138 Bologna Italy [4]Center of Study and Research on Obesity, Department of Medical Biotechnology and Translational Medicine, University of Milan, via Vanvitelli 32, 20129 Milan, Italy [5]Fondazione Toscana Gabriele Monasterio, via Moruzzi 1, 56124 Pisa, Italy [6]Department of Surgical, Medical, Molecular Pathology and Critical Care Medicine, Division of Pathology, Pisa University Hospital, 56124 Pisa, Italy

[7] First authors equal contribution.

*Corresponding author.

**Corresponding author.

E-mails: federica.larosa@cnr.it (F. La Rosa), mariaangela.guzzardi@cnr.it (M.A. Guzzardi), M.Mercedes.Pardo@uv.es (M. Pardo-Tendero), monica.barone@unibo.it (M. Barone), chiara.ruocco@unimi.it (C. Ruocco), gabriele.conti12@unibo.it (G. Conti), daniele.panetta@cnr.it (D. Panetta), dariariabitch@cnr.it (D. Riabitch), silvia.bernardi@cnr.it (S. Bernardi), asso@ftgm.it (A. Giorgetti), daniela.campani@med.unipi.it (D. Campani), daniel.monleon@uv.es (D. Monleon), enzo.nisoli@unimi.it (E. Nisoli), patrizia.brigidi@unibo.it (P. Brigidi), patricia.iozzo@cnr.it (P. Iozzo).

Abbreviations: AA, aminoacids; AT, adipose tissue; BCAA, branched-chain amino acids; BAT, brown adipose tissue; BMI, body mass index; CT, computed tomography; FMT, fecal matter transfer; GF, germ-free; GM, gut microbiota; NMR, nuclear magnetic resonance; PET, positron emission tomography; pgWAT, perigonadal white adipose tissue; PVAT, perivascular adipose tissue; scWAT, subcutaneous white adipose tissue; TCA, tricarboxylic acid; TMA, trimethylamine

Received January 9, 2025 • Revision received March 28, 2025 • Accepted April 22, 2025 • Available online 25 April 2025

https://doi.org/10.1016/j.molmet.2025.102157

1. INTRODUCTION

Childhood and adolescent obesity are major public health concerns, associated with severe health consequences, including prediabetes, type 2 diabetes (T2D), cardiovascular disease, and premature mortality [1–3]. Since the 1980s, the prevalence of obesity and T2D in these age groups has increased dramatically, leading to an alarming rise in early-onset complications and death during adulthood [1–6].

Children with obesity are at a high risk of becoming metabolically unhealthy adult, often exhibiting sex-specific complications [7]. Despite lifestyle interventions, the resilience of obesity and its metabolic abnormalities persists, even after significant weight loss. This highlights the urgent need for effective preventive strategies, particularly during early life - a critical window for long-term programming. The gut microbiota has emerged as a promising therapeutic target due to its key role in regulating adipose tissue (AT) function, glucose metabolism, and overall metabolic health. Early life is especially crucial, as it represents the period of gut microbiota colonization and stabilization (between 3 and 5 years of age) and AT development, which collectively influence metabolic outcomes later in life. Recent preclinical imaging studies (μPET-CT) have revealed that early metabolic stress induces sex-specific AT phenotypes, with diabetogenic effects in females and obesogenic effects in males, accompanied by distinct microbiota signatures [8,9].

We hypothesized that the early-life microbiota of children with obesity induces persistent metabolic imprinting on AT and glucose homeostasis. If this imprinting becomes irreversible after infancy, regardless of subsequent microbiota changes, the window for effective microbiota-mediated interventions could be drastically narrowed. While testing this hypothesis in humans would require decades of follow-up and face numerous confounding factors, mouse models offer a practical alternative, as the transition from infancy to adulthood occurs within 3–4 months, allowing for mechanistic investigations and direct access to tissues. Fecal microbiota transplantation (FMT) studies have shown that gut microbiota influences AT dysfunction [10], including changes in radiodensity, glucose uptake, and thermogenic activity, in addition to intestinal (cecum) glucose, lipid, and amino acid metabolism [11–14]. Additionally, microbial metabolites, such as branched-chain amino acids (BCAAs), play critical roles in linking gut and adipose metabolism [15,16]. However, existing FMT studies have primarily focused on adult donors and short-term outcomes, leaving the long-term effects of childhood microbiota implantation unexplored [13].

This study aimed to investigate the long-term consequences of early-life FMT from preschool children with obesity on AT function and glycemic control in sex-matched adult mice. We provide the first evidence that a single FMT in infancy programs a diabetogenic, inflammatory AT phenotype in adult female mice, and an obesogenic phenotype in adult male mice. Shared fecal metabolic mediators, namely metabolites showing associations between donor and recipient after FMT were identified, suggesting potential mechanisms underlying these persistent metabolic effects.

2. MATERIALS AND METHODS

2.1. Children donors

We used FMT from 5-year-old child donors, stratified according to BMI and weight-to-length percentile scores, to colonize (*i.e.*, humanize) sex-matched GF mice in early life (Figure 1A–C). Children donors (n = 20, 50% females/males) [17] were a subset of the Pisa birth cohort (PISAC), which includes 90 families with children (42/48 F/M) born and recruited between 2012 and 2014 [18]. The characterization at 5 years included a dietary assessment [19,20] with a validated food frequency questionnaire (FFQ), consisting of 53 commonly used food items, to calculate weekly grams of foods, and daily calories from nutrients according to the Food Composition Database for Epidemiological Studies in Italy (BDA) and the Food Composition Tables (CREA), assuming standard age-appropriate portion sizes [21–23]. BMI and weight-to-length percentiles were calculated using the Children's Growth Chart Online Calculator by the CDC (2–20 years: Weight for Stature Percentile). Donors were categorized based on a BMI cut-off of 16.8 kg/m^2 (85th percentile) into a lean group and a group with obesity, comprising boys (n = 5 each) and girls (n = 6 lean, 4 with obesity).

2.2. Animal recipients

We studied 60 germ-free C57BL/6 mice, aged 4–5 weeks, obtained from Charles River Laboratories, Calco (LC), Italy. One male mouse died upon arrival, and five were excluded for urinary tract infection (3 from obese, 2 from lean donors). Mice were housed in individually ventilated cages, three per cage, in a controlled environment with 12-hour light/dark cycles at a room temperature of 22 °C. Mice were fed a standard low-fat diet (53.5% carbohydrate, 3% fat, 18.5% protein; autoclavable 4RF21, Mucedola, San Donato Milanese, MI, Italy) throughout the study and had *ad libitum* access to food and water. As summarized in Figure 1C, GF mice (n = 3 sex-matched replicates/donor, cohoused) were colonized in early life (1 month of age). GF mice were randomly allocated to experimental groups. After one-week of acclimatization, single oral gavage using sterile plastic feeding tubes (20ga x 30 mm, Biological Instruments S.N.C., Besozzo, VA, Italy) was performed to transfer suspensions of 150 μL of children's faecal samples (0.1 g of faecal material diluted in 770 μL sterile PBS solution) into sex-matched mice (at a 1:3 ratio, *i.e.*, three replicate mice per each donor). A total of 33 mice received samples from lean donors (15 males and 18 females) and 26 mice received samples from donors with obesity (14 males and 12 females) and completed the study. All procedures were conducted in a laminar flow biosafety cabinet sterilized with ultraviolet light (UV) and decontaminated with an alcoholic disinfectant solution containing 0.5% chlorhexidine gluconate and ethyl alcohol (Neoxidina Alcolica "S" 1 lt). The investigator, who wore a sterile gown, gloves, face mask, and hair cover, was the same for all procedures. Cages, litter, water, and food were sterilized by autoclaving prior to cage changes and replaced with sterile materials every week for 6 months. Body weight and food intake were monitored weekly. Individual food intake (g/day) was determined by measuring the difference between the remnant and served food (120 g/cage), normalized to the number of days and mice in each cage. The feed efficiency ratio (FER) was calculated as the ratio of body weight gain (g) to food intake (g) during the observation period, representing the efficiency of converting consumed food into body mass [24,25]. Cumulative body weight, food intake, and FER are expressed as areas under respective curves (AUC_{BW}, AUC_{FI}, AUC_{FER}).

We monitored fecal microbiota trajectories at 1, 4, 9, 15, 19, 22, and 23 weeks after FMT, and intermediary effects on fecal metabolites at 1, 15 and 23 weeks. At adult age (~6 months), we assessed the organ-specific glucose metabolism by PET-CT imaging and the phenotypes (histology) of AT, which included BAT, perivascular (PVAT), perigonadal (pgWAT) and subcutaneous depots (interscapular = $scWAT_i$, abdominal = $scWAT_{ab}$), the amino acid profile of BAT and pgWAT, and the intestinal expression of genes regulating gut-barrier permeability, and mitochondrial function in the cecum. The cecum represents a site of significant microbiota–nutrient interaction in mice. Previous studies in microbiota-depleted rodents

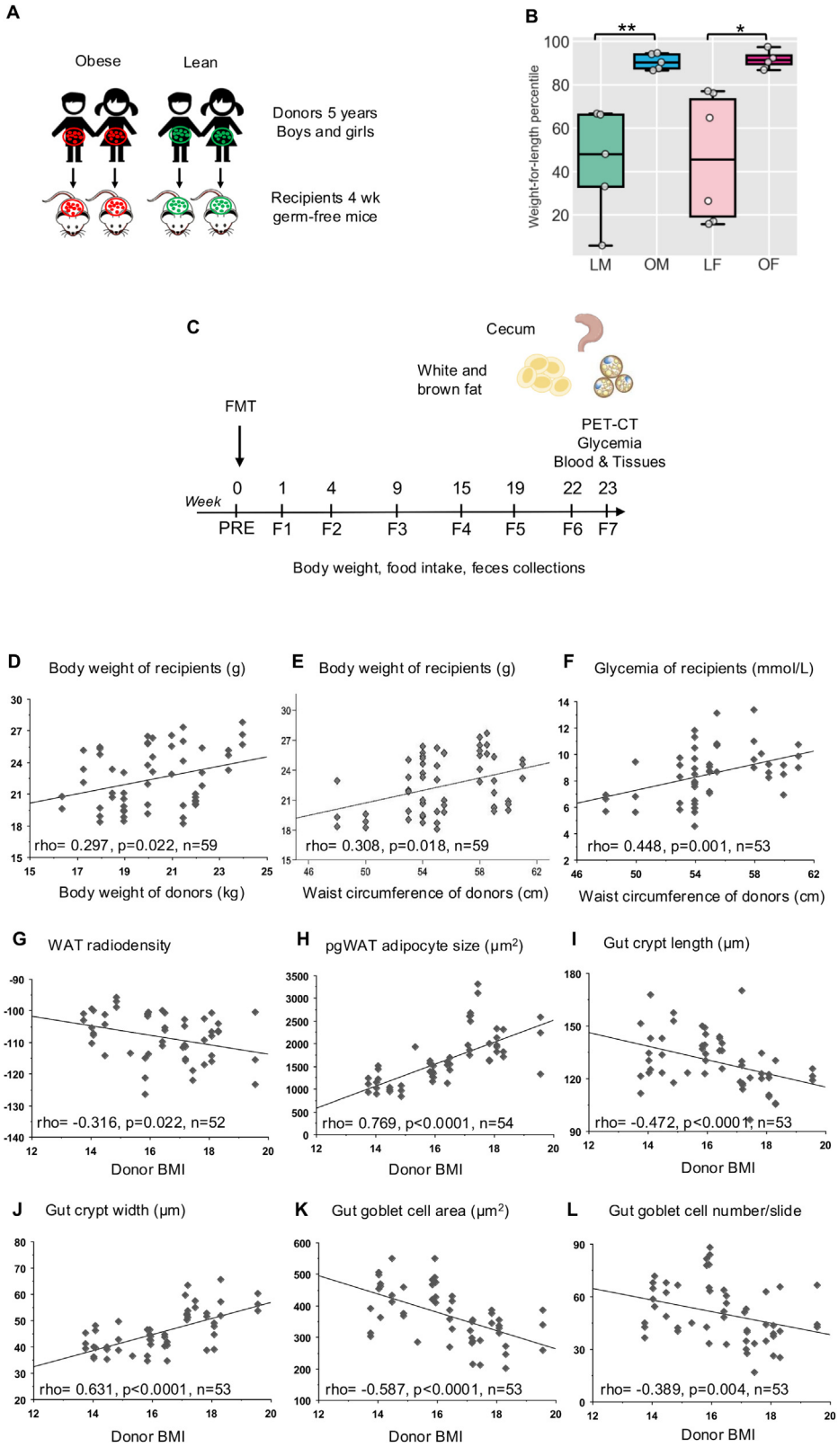

Figure 1: Transfer of gut microbiota from children to mice confers a correlated phenotypes. Study design: sex-matched FMT was performed from preschool children with obesity (red) or without obesity (green) (panel A), with corresponding weight-for-length percentile shown in panel B. Four-week-old germ-free (GF) mice received FMT and were monitored until 6 months of age (23 weeks post-FMT), as shown in panel C. (D–L) Phenotypic correlations. Regression analyses showing significant correlations between donor anthropometric measures and recipient characteristics. Spearman's correlation coefficients, p values, and sample size are indicated in each panel, highlighting proportional relationships between donor and recipient parameters, independent of stratification. A comprehensive list of correlations is provided in Table S1.

have shown that cecum enterocyte metabolism [26] contributes to systemic glucose regulation, with cecum glucose uptake related to BAT metabolism [11].
The study protocol was approved by the Italian Ministry of Health (decree n 464/2018-PR).

2.3. PET-CT imaging

Adult animals were fasted for 7 h before imaging. Anaesthesia was induced using 3–4% (v/v) isoflurane and maintained with 1–2% isofluorane (IsoFlo®, Abbott Laboratories, Chicago, IL, USA). After determining body weight and fasting glycemia, imaging was conducted using a dedicated small animal PET-CT tomograph (IRIS PET/CT, Inviscan SAS, Strasbourg, France). A low-dose CT scan (total scanning time 20 s, voltage 80 kVp, total current 18 mAs) was acquired, followed by ^{18}FDG intraperitoneal injection, and whole-body dynamic PET scanning lasting 100 min, and then a high-resolution CT (65 kV, 112 s, 112 mAs). Breath frequency was monitored. Blood glucose levels were measured from tail blood using a glucometer (OneTouch, Johnson&Johnson Medical SpA, Italy) at 30-, 60-, and 90-minutes post-injection.
All CT images were reconstructed using cone-beam filtered back-projection (FBP) with correction for geometric misalignments, spectral hardening, and ring artifacts, then exported to DICOM format. High-resolution CTs had a matrix of 600 × 600 x 1458 voxels, with an isotropic sampling rate of 76.95 microns. PET data were corrected for dead time and radioactive decay, reconstructed using the three-dimensional iterative ordered-subset expectation-maximization (3D-OSEM) algorithm, and co-registered to CT images using dedicated software (AMIDE Medical Image Data Examiner v.1.0.5).
Regions of interest were manually drawn on PET images corresponding to BAT, scWAT$_{ab}$, pgWAT, and cecum by using dedicated software (AMIDE Medical Image Data Examiner v.1.0.5). Respective activity levels in late time-frames were divided by the injected dose per gram of body weight (%ID/g or standardized uptake value, SUV) reflecting the fractional tracer extraction rate constant, and multiplied by glycemia to estimate regional glucose uptake rates (GU) [9]. High-resolution CT images were used to measure BAT and total AT volumes, using a semi-automatic segmentation procedure with Seg3D v2.4.4 software, and BAT, AT, and cecum mean radiodensities, expressed as Hounsfield units (HU), were assessed using ImageJ software (ImageJ 1.53k, Wayne Rasband and contributors, National Institutes of Health, USA, https://imagej.nih.gov/ij).

2.4. Adipose tissue and cecum histology

BAT, scWAT$_i$, pgWAT and cecum samples were fixed in 10% neutral buffered formalin, dehydrated in ethanol, included in paraffin using the Donatello Diapath automatic tissue processor (Martinengo, Bergamo, Italy), sectioned (HistoCore Autocut, Leica BioSystems microtome) at a thickness of 4 μm (AT) or 3 μm (cecum), and stained with hematoxylin and eosin using the automated Dako CoverStainer (Santa Clara, CA, USA). Sections were documented by using an Olympus BX43 microscope connected to an Olympus DP20 digital camera and cellSens Dimension Ver1.5 Imaging Software (Olympus Corporation, Shinjuku Monolith, 3-1, Nishi Shinjuku 2-chome, Shinjuku-ku, Tokyo, Japan). Sections were analyzed by a blinded operator using ImageJ software (ImageJ 1.53k, Wayne Rasband and contributors, National Institutes of Health, USA, https://imagej.nih.gov/ij).
Six histological BAT and scWATi section, and three histological sections of the cecum from each animal were selected and analysed. BAT sections were documented at 20× magnification, the color scale was converted to an 8-bit grayscale image with 256 intensity levels (black and white = 0 and 255), and the image was binarized (white for lipid droplets and black for the remaining BAT) to compute respective percentages. Within BAT, larger adipocytes surrounding vessels (perivascular AT, PVAT) were quantified on a scale of 1 (very low) to 6 (high) around three vessels and averaged. Additionally, crown-like structures (CLS) and inflammatory foci in scWAT$_i$ were quantified at 20× magnification. In pgWAT, three images per animal were analysed at 40× magnification. Cell area of 10 adipocytes per image (n = 30 adipocytes/animal) was quantified using cellSens Dimension Ver1.5 Imaging Software and averaged. The number of adipocytes per image was estimated using ImageJ software (version 1.46r, https://imagej.nih.gov/ij).
For the cecum, the analysis focused on the mucosa, submucosa, and muscularis externa layers of the cecum. In the mucosa, crypts and goblet cells were counted in each image. Three crypts per image were analyzed at 20× magnification for apical and basal length, total crypt length, crypt width and transversal area. Additionally, the depth and number of open spaces between crypts were measured. The area of three goblet cells per image was quantified at 40 × magnification. The thickness of the submucosa and muscularis externa (including circular and longitudinal sublayers) was assessed in three zone per image and averaged.

2.5. Adipose tissue amino acids (AA)

Free AA concentrations in BAT and pgWAT were measured in samples from 12 mice (equal numbers of males and females; three per experimental group, one per littermate triplet, selected based on sample quality). Quantification was performed by cation-exchange chromatography with post-column ninhydrin reaction and spectrophotometric detection using a Biochrom 30+ Amino Acid Analyzer (Biochrom Ltd, ERRECI s.r.l Pieve Emanuele, Italy), as previously described [27]. Analyses were conducted using three samples per group. Samples were weighed and homogenized in 250 μL of 0.1% Triton X-100 loading buffer (Sigma Aldrich, Milan, Italy) using cold sonication for 30 s [27]. Homogenates were mixed with a 5% sulphosalicylic acid (SSA) deproteinization reagent (1:1), containing L-Norleucine as an internal standard (final concentration: 250 μmol/L, Sigma Aldrich, Milan, Italy). Samples were incubated at 4 °C for 30 min, then centrifuged at 10,000×*g* for 5 min at 4 °C.
To completely remove protein fractions, the supernatants were filtered through 0.22 μm filter columns (Millipore, Milan, Italy) by centrifugation at 12,000×*g* for 10 min at 4 °C. Calibration standard solutions (final concentration for each AA: 250 μmol/L; Biochrom Ltd, Cambridge Research Park, UK) were processed with the same L-Norleucine SSA 5% buffer to ensure pH consistency during loading. Both standards and samples, kept cold during the procedure, were injected into the analyzer (60 μL per sample).
Amino acid levels were detected spectrophotometrically at 440 nm and 570 nm after a post-column reaction with ninhydrin under controlled conditions (135 °C). Separation of amino acids was achieved using cation-exchange chromatography, with a negatively charged resin ensuring positive charge retention of the amino acids at low pH.

2.6. Gene expression of cecum

Quantitative RT-PCR was performed on samples from 12 mice (equal numbers of males and females; three per experimental group, one per littermate triplet, selected based on sample quality) as previously described [28]. Briefly, total RNA was isolated from cecum samples using the RNeasy Mini Kit (Qiagen, Milan, Italy) and treated with DNase according to the manufacturer's protocol. cDNA was synthesized using an iScript cDNA Synthesis Kit (Bio-Rad Laboratories, Segrate, Italy) and

amplified by real-time quantitative PCR with iTaq Universal SYBR Green SuperMix (BioRad Laboratories) on a CFX Connect Real-Time PCR System (Bio-Rad Laboratories). The expression of gut permeability genes, zonulin-1 (ZO1), claudin 4, and claudin 7, as well as e-Cadherin, an adherence junction protein [29], and of mitochondrial genes peroxisome proliferator-activated receptor γ coactivator 1α (PGC-α), the master regulator of mitochondrial biogenesis, transcription factor A (Tfam), involved in mitochondrial DNA replication and repair, and components of the electron transport chain, cytochrome c oxidase subunit IV (COX IV) and cytochrome c (Cyt c) was assessed [30]. Primers were designed using Primer3 (version 0.4.0) software, and their sequences are listed in Table S6. The cycle threshold (CTh) at which the various transcripts were detectable was compared with the CTh of housekeeping genes to obtain the ΔCT value. Gene expression levels were calculated using the $2^{-\Delta\Delta CT}$ method, where $\Delta\Delta$CT represents the difference between the ΔCT of the treatment group and the ΔCT of the control group.

2.7. Fecal microbiota profiling

2.7.1. Microbial DNA extraction

A total of 398 stool samples were collected from mice at various stages. Microbial DNA was extracted from mouse stool samples using the QIAamp® Fast DNA Stool Mini kit (QIAGEN, Hilden, Germany). Briefly, 250 mg of fecal samples were suspended in 1.4 ml of ASL buffer, added with four 3-mm glass beads and 0.5 g of 0.1-mm zirconia beads (BioSpec Products, Bartlesville, OK, USA), and homogenized using a vortex. The samples were incubated at 95 °C for 5 min, followed by chemical and mechanical lysis using a FastPrep instrument (MP Biomedicals, Irvine, CA, USA) with two bead-beating steps at 5.5 movements/sec for 45 s, with a 5-min incubation on ice between treatments. The samples were then vortexed for 15 s, and stool particles were pelleted by centrifugation at 13,000 rpm for 1 min. Half of an InhibitEX tablet (QIAGEN) was added to each sample to remove inhibitors. After 1-min incubation, two centrifugation steps were performed at 13,000 rpm for 3 min. DNA purification was completed using the column-based method provided in the QIAamp® Fast DNA Stool Mini kit (QIAGEN), following the manufacturer's instructions. The extracted DNA yield and quality were assessed with a NanoDrop ND-1000 spectrophotometer (NanoDrop Technologies, Wilmington, DE, USA).

2.7.2. 16S rRNA gene sequencing and bioinformatics

The V3—V4 hypervariable regions of the 16S rRNA gene were amplified in 50 µl volume using KAPA HiFi HotStart ReadyMix and the 341F and 785R primers with Illumina adapter overhang sequences, as described in Barone et al. [31]. For library preparation, amplicons were purified using a magnetic bead-based system (Agencourt AMPure XP, Beckman Coulter, Brea, CA, USA) and indexed using Nextera technology through limited-cycle PCR. Indexed libraries were pooled at 4 nM, denatured with 0.2 N NaOH, and diluted to 5 pM. Sequencing was performed on an Illumina MiSeq platform using a 2 $\times$ 250 bp paired-end protocol according to the manufacturer's instructions (Illumina, San Diego, CA, USA).

Bioinformatic analyses followed Barone et al. [31]. Raw amplicons were processed by combining PANDASeq [32] and QIIME2 [33]. Raw sequences were quality-filtered using USEARCH11 [34], and high-quality reads were binned into amplicon sequence variants (ASVs) using DADA2 [35] after removing chimeras. The SILVA database v138.1 [36] was used for taxonomic assignment through a hybrid method involving VSEARCH and a Naïve-Bayes classifier trained on the SILVA 138.1 database [35], processed with RESCRIPt [37], according to QIIME q2-feature-classifier plugin indications [38]. QIIME 2 version 2023.5 was used for taxonomic and diversity computation. Alpha and beta diversity were calculated with the "qiime diversity core-metrics-phylogenetic" plugin. Alpha diversity was evaluated using Shannon entropy index and the number of observed features (ASVs). Beta diversity was estimated by computing weighted and unweighted UniFrac distance, used as input for principal coordinates analysis (PCoA). The obtained ASVs were filtered for a prevalence in samples of $\geq$0.2% in at least 1/6 of all samples and used to generate bar plots and box plots. PCoA, bar plots and box plots were constructed using the R packages "vegan" (http://www. cran.r-project.org/package = vegan) and "MicrobAIDer" [39]. Statistically significant differences in alpha diversity and relative taxon abundance between groups were evaluated by Wilcoxon test ($p \leq 0.05$).

2.8. Fecal and plasma metabolites by proton NMR spectroscopy

2.8.1. Sample collection and preparation

Stool samples were collected at 1, 15, and 23 weeks post-transplant. Blood samples were collected at the end of study protocol, immediately following the PET-CT session. Fecal samples were suspended in Milli-Q water (100 µL) and centrifuged (14,800 rpm, 5 min) three times consecutively to obtain extracts. A mixture of 20 µl of plasma and 2 µl of phosphate buffer with trimethylsilyl propanoic acid and deuterated water was transferred into a 1-mm high-quality nuclear magnetic resonance (NMR) individual tube.

2.8.2. NMR spectroscopy

Proton NMR spectra were recorded using a Bruker Avance DRX 600 spectrometer equipped with a triple resonance 1H/13C/31P probe. The nominal temperature of the sample was maintained at 310 K. A single pulse presaturation experiment was acquired in all samples. The number of transients was 256, collected into 65 k data points. Spectral chemical shift referencing was performed on the alanine CH3 doublet signal at 1.475 parts per million (ppm). Spectra were processed using MestReNova 8.1 (Mestrelab Research S.L., Spain) and transferred to MATLAB (MathWorks, 2012) using in-house scripts for data analysis. The chemical shift region, including resonances from 0.50 to 4.50 ppm (the aliphatic region) and 5.20—10.00 ppm (the aromatic region), were investigated.

2.8.3. Data analysis

Metabolite spin systems and resonances were identified using literature data and the Chenomx resonances database (Chenomx NMR 7.6). Spectra were normalized to the total aliphatic spectral area (excluding lipids) to eliminate differences in metabolite concentration. NMR peaks were integrated and quantified using semi-automated in-house MATLAB peak-fitting routines. Final metabolite levels were calculated in arbitrary units as peak area normalized to the total spectral area. Chemometric analysis was performed with PLS ToolBox 8.0 (Eigenvector Inc.) in MATLAB. PLS-DA was applied to maximize the separation between samples and to identify discriminant patterns. Spectral regions with high VIP coefficients during PLS-DA were identified as contributing significantly to class separation, while those with very small VIP coefficients provided minimal contribution to classification.

2.9. Circulating markers

Blood was centrifuged for 10 min at 3000 rpm, and plasma was stored at −80 °C. Levels of leptin, resistin, insulin, C-peptide, MCP1, IL6, and TNF-alpha were simultaneously determined using a multi-analyte

panel based on Luminex® xMAP® technology (Milliplex map kit, CAT N# MMHMAG-44K, Merk Life Science S.r.l. Milan, Italy).

2.10. Statistical analyses

Body weight, food intake, circulating markers, imaging parameters, and single metabolites were analysed using the IBM SPSS Statistics Ver.26 software package (SPSS, Chicago, IL, USA) and represented in box plots made by Seaborn, Python 3.8. A non-parametric approach was adopted for group comparisons of these variables by Mann—Whitney test between sex-matched obese vs. lean cases. Unpaired t-testing was preferred to support AA and gene expression results, which were available in a subset of 10—12 mice, and compared by using Prism 6.0 software (GraphPad Software, Inc.), estimating a *post-hoc* power of 0.55% (e.g., isoleucine) to 0.96% (e.g., leucine). Data are presented as means ± SEM. Statistical significance was set at p value < 0.05.

2.11. Multi-omics data integration

To elucidate the complex relationships within biological systems, this study employed a comprehensive multi-omics approach. Data from different metrics at 23 weeks were organized into six distinct layers, which included fecal metabolome, plasma metabolome, body parameters, intestinal morphology and metabolism, AT morphology and metabolism, and microbiota composition (Table S4).

The Kruskal—Wallis test was used for each layer to evaluate the four phenotypes, identifying significant parameters for subsequent analysis. The filtered layers were integrated and analyzed using the R MixOmics package DIABLO (Data Integration Analysis for Biomarker discovery using Latent cOmponents) [40], an advanced tool for the integration of multi-omics datasets. An initial DIABLO model was generated using the "block.splsda(a)" function with an arbitrarily high number of components (ncomp = 7) to match the lowest variable count in one of the layers. Subsequently, component tuning, and feature selection were performed to optimize the parameters of the final model. The "perf(a)" function was executed with a 10-fold cross-validation repeated 100 times to determine the optimal number of components. The "tune.block.splsda(a)" function, also with 10-fold cross-validation repeated 100 times, was used for variable tuning selection, identifying key features of the final DIABLO model. The final DIABLO model was constructed based on the optimized parameters and selected features. Results were visualized using appropriate MixOmics R functions. This multi-omics integration approach allowed for the identification of key biomarkers and relationships within the biological data, providing a comprehensive understanding of the underlying biological systems.

3. RESULTS

3.1. Children's FMT imprints gut, adipose, and metabolic phenotypes in recipient mice persistently

Direct associations were observed between the phenotypes of child donors and recipient mice. The body weight or waist circumference of donors correlated significantly with that of recipients from two weeks post-FMT and persisted into adulthood (Table S1, Figure 1D-E). Higher donor BMI or waist circumference predicted larger adipocyte size, increased lipid content and inflammation in AT, as well as greater intestinal crypt and goblet cell size in mice (Table S1, Figures 1G-1L). These donors also influence higher glucose levels in adult recipient mice (Figure 1F). Considering that FMT was conducted in early-life mice and their outcomes were measured in adulthood, the finding of significant correlations suggests a strong and persistent influence of the donor microbiota on the recipients' phenotypes.

3.2. A single early-life FMT induces obesogenic and diabetogenic profiles in adulthood

Recipient mice were grouped based on the FMT donor's characteristics: female or male children with obesity (OF and OM) or without obesity (lean; LF and LM) (Figure 1A). Glucose levels in adulthood were significantly higher (+23%) in OF compared to LF mice, with a mild trend observed in OM (Figure 2C). This suggests that microbiota from children with obesity, particularly females, confers a pronounced diabetogenic risk. In vivo PET imaging (Figure 2A) revealed greater glucose uptake in the tested AT depots in OF mice (Figure 2F). This was accompanied by a higher frequency of inflammatory loci and crown-like structures (CLS) (Figures 2B, 2D-2E) but no significant lipid excess in $scWAT_i$ compared to LF mice (Figure 2G). Conversely, OM mice exhibited histological tendency towards lipid accumulation in scWATi, without significant increases in inflammation or glucose uptake (Figure 2D—G), and significantly larger total body AT volume and lower CT radiodensity, indicative of greater fat content, which was not observed in OF mice (Figure 2H,K). Interestingly, BAT in OM mice was marginally larger and visually whiter compared to LM mice (not statistically significant) (not shown), with a significant increase in glucose uptake (Figure 2J,I). This finding supports the hypothesis that glucose uptake in thermoneutral BAT facilitates *de novo* lipogenesis and the provision of glycerol-3-P supply for triglyceride synthesis [41].

Visceral fat depots, including pgWAT and PVAT, displayed approximately 100% larger adipocytes (pgWAT) or adiposity expansion (PVAT) in OF and OM mice compared to their lean counterparts (Figures 2M—2N). Leptin levels tended to be higher (371 ± 126 vs 186 ± 38 pg/ml), while resistin levels were markedly lower in OM vs LM (946 ± 157 vs 2124 ± 542 pg/ml, p = 0.008 by Mann—Whitney test). These hormonal alterations were not observed in OF mice.

In both male and female mice, lower CT radiodensity was strongly correlated with greater histological triglyceride accumulation in BAT (as lipid droplet occupation) and WAT (as increased adipocyte size) (Fig. S1). Additionally, reduced radiodensity in BAT (indicative of "whitening") and WAT was strongly associated with elevated circulating levels of insulin and C-peptide, in male and female mice, and leptin in male mice (Fig. S1), which are well-established markers and drivers of adiposity and lipogenesis. In males, leptin levels tended to be also linked to BAT volume and glucose uptake, while in females, glucose uptake in scWAT was correlated with the presence of inflammatory foci and crown-like structures in $scWAT_i$ (Fig. S1).

We further investigated eating behavior as a potential contributing factor to the observed AT phenotypes. In both sexes, food intake and body weight progressively increased until 15—17 weeks of age (approximately 4 months in mice, analogous to 20—25 years in humans) and stabilized thereafter (Figure 3). OM mice consumed fewer calories than LM mice during the pre-adult period (Figure 3A); however, their weight gain was consistently higher (Figure 3B), indicative of a more efficient conversion of food into body mass, as reflected by a higher feed efficiency ratio (FER) (Figure 3C). In contrast, OF mice consumed more calories than LF mice starting from the third week post-FMT (Figure 3D), but their weight gain and FER were comparable to those of LF mice (Figure 3E—F).

3.3. Impact of fecal microbiota on BCAA levels in ATs

BCAA levels in pgWAT were comparably higher in both OF and OM than LF and LM mice, consistent with their similar pgWAT phenotype (Figure 4A—C). Conversely, BCAA levels in BAT were hundreds of times higher in OM than LM mice and other groups (Figure 4E—G). Notably, this effect was not observed in female recipients (Figure 4E—G). An aminogram analysis revealed only subtle changes in the free amino acid

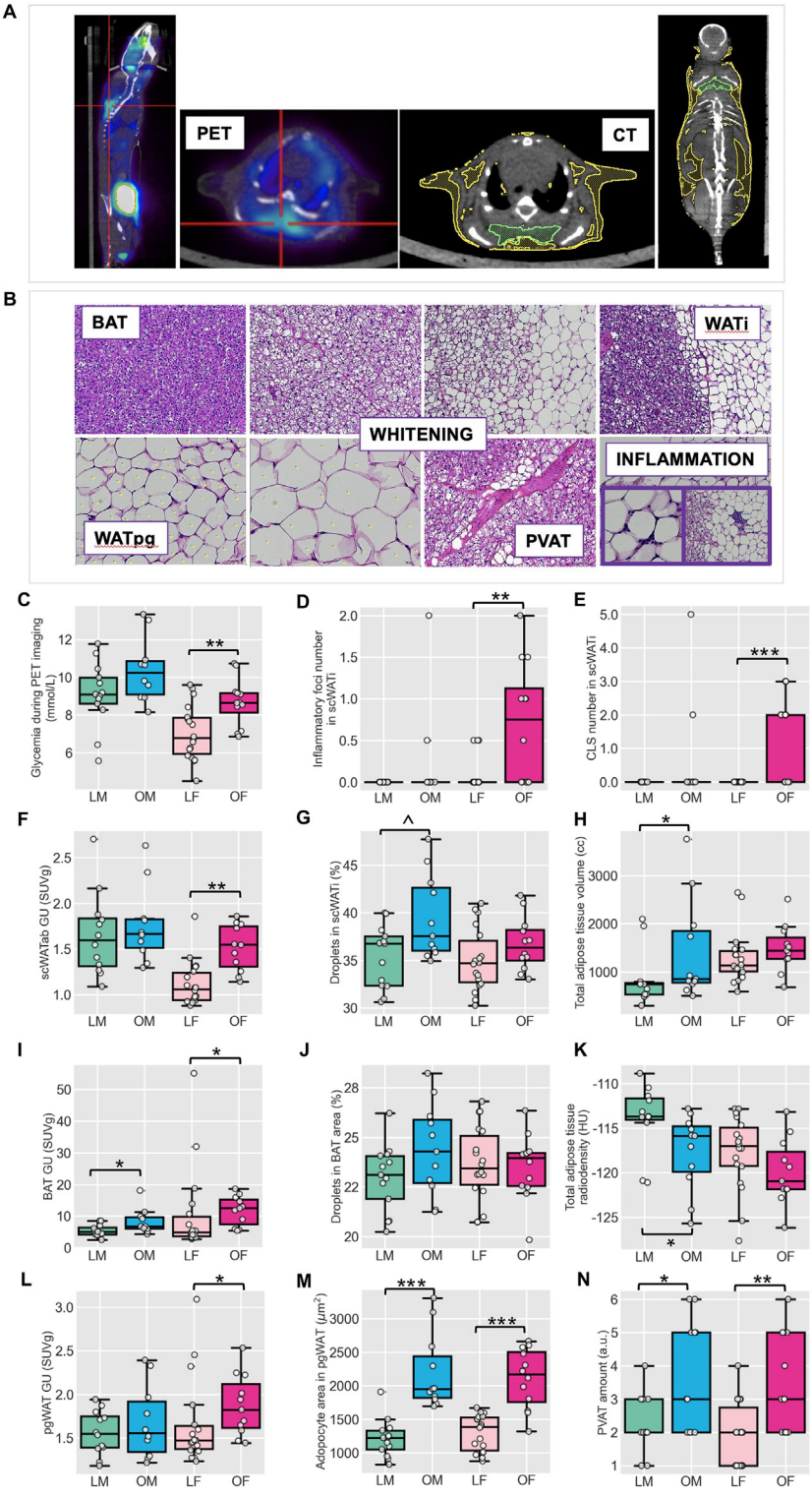

Figure 2: Adipose tissue (AT) metabolic responses to early life FMT in mice: obesogenic and diabetogenic profiles modulated by donor phenotype. (A) Representative PET and CT images showing *in vivo* assessment of adipose tissue. PET images (left) show FDG uptake in sagittal and transaxial planes, with interscapular BAT highlighted (cross mark). Glucose uptake is expressed as standardized uptake value multiplied by glucose values (SUVg). CT images are segmented to distinguish BAT (green contour) from WAT (yellow contour), with extracted tissue volumes (cc) and radiodensity values (Hounsfield units, HU). (B) Representative histological sections used to quantify adipocyte size, lipid occupancy, inflammatory loci, and crown-like structures (CLS) *ex vivo*. (C—E) Blood glucose levels and inflammatory infiltrates in subcutaneous interscapular WAT ($scWAT_i$). (F-G, I-J, L-N) Adipose tissue morphometry and glucose uptake in abdominal subcutaneous WAT (scWAT), perigonadal WAT (pgWAT), interscapular BAT, and perivascular adipose tissue (PVAT). (H, K) Whole-body adiposity measurements. Group comparisons were performed within each sex using Mann—Whitney U tests. Data are shown as individual points with boxplot. Significance is indicated as follows: *$p < 0.05$; **$p < 0.01$; ***$p < 0.0001$; ^$p < 0.07$. Recipient mouse groups are named according to donors' phenotype: lean male (LM), lean female (LF), obese male (OM), and obese female (OF).

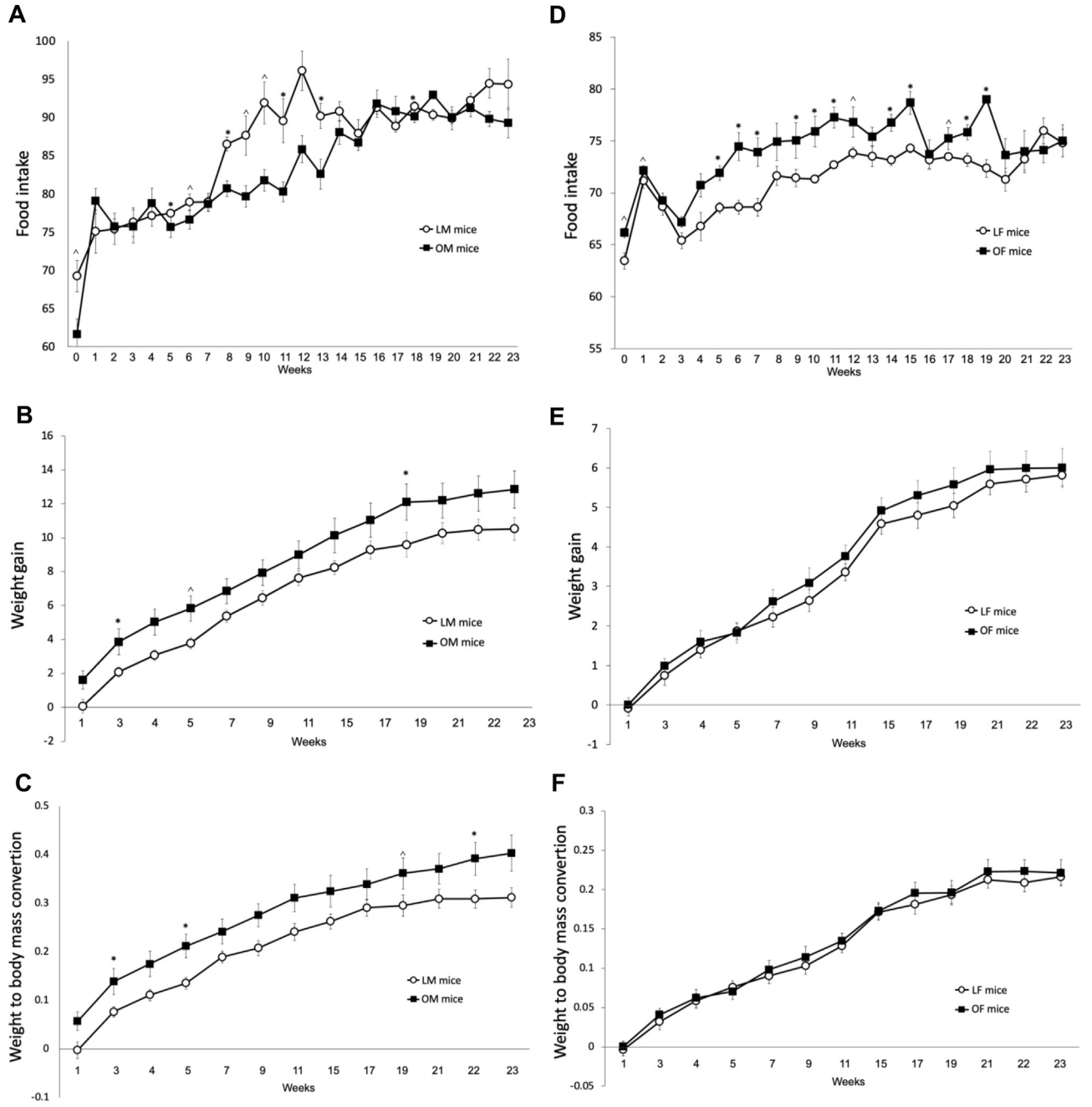

Figure 3: Eating behavior and body growth in recipient mice following early-life FMT. (A—F) Longitudinal observations of food intake, weight gain, and feed efficiency ratio are shown in male (A—C) and female (D—F) mice recipients of FMT from sex-matched children without and with obesity. Group comparisons were performed at each time point within sex using Mann—Whitney U tests. Significance is indicated as * $p < 0.05$; ^$p < 0.07$. Recipient groups are designated according to donor phenotype: lean male (LM), lean female (LF), obese male (OM), and obese female (OF).

profile of pgWAT across groups (Table S2). Instead, BAT in OM mice displayed a marked increase in most amino acids (Table S3). An exception was taurine, which was deficient in the pgWAT of OM mice (Figure 4D) and in both pgWAT and BAT of OF mice (Figures 4D, 4H). This taurine deficiency aligns with its association metabolic dysfunctions [42].

3.4. Gut microbiota dynamics

The reduction of microbiota alpha diversity in recipients compared to donors is a commonly used metric to evaluate FMT engraftments [43,44]. In this study, the reduction in diversity was consistent with prior findings in the field. Shannon index was 25% lower in recipient mice compared to donors one-week post-FMT ($p \leq 0.001$, Wilcoxon test; Figure 5A), and the number of observed features (ASVs, not shown) was 59 ± 4 in child donors vs 25 ± 2 in FMT mice. Beta diversity analysis revealed significant differences in GM composition between groups and across timepoints ($p \leq 0.05$, permutation test with pseudo-*F* ratio; Figure 5B, Fig. S2), with sex emerging as a key factor driving microbial community segregation, regardless of donor BMI phenotype.

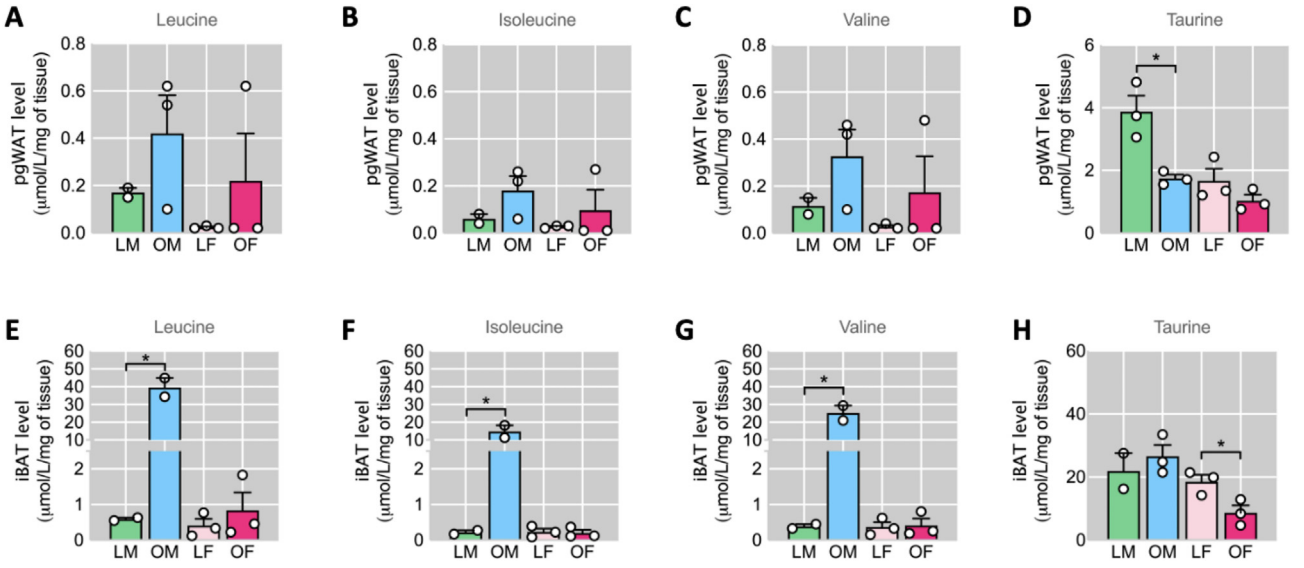

Figure 4: Differential impact of early-life FMT on branched-chain amino acid (BCAA) levels in adipose tissues of recipient mice. BCAA and taurine levels measured in perigonadal white adipose tissue (pgWAT, panels A—D) and interscapular brown adipose tissue (BAT) (panels E—H). A full list of the amino acid spectrum is given in Tables S2—S3. Unpaired t-tests were conducted within each sex group. Sample size and distribution are shown by individual points in each histogram. *$p < 0.05$. Recipient groups are labeled according to donor phenotype: lean male (LM), lean female (LF), obese male (OM), and obese female (OF).

Taxonomic analysis revealed significant sex- and BMI-dependent variations in GM composition among FMT recipients. FMT mice primarily harbored Verrucomicrobiota (24.6%) and Bacteroidota (21.5%). Female FMT recipients (LF, OF) exhibited higher *Akkermansia* and *Parabacteroides*, whereas males (LM, OM) showed increased *Bacteroides* and *Coprobacillus* ($p \leq 0.05$, Figure 6A). *Collinsella* and *Lachnospiraceae* NK4A136 group abundance was significantly greater in LF. Obese FMT recipients displayed an increase in *Paraprevotella*, particularly at later timepoints (e.g., week 23, $p = 0.008$), consistent with its association with obesity-related GM configurations. Conversely, lean groups were enriched in *Eisenbergiella* and the *Lachnospiraceae NK4A136 group* ($p \leq 0.05$, Figure 6B). These findings underscore the influence of donor characteristics on shaping GM ecosystems, highlighting their role in modulating long-term metabolic and intestinal development. For further details on additional results, please refer to the Supplementary Material.

3.5. Gut histology, permeability, and mitochondrial biogenesis in FMT recipients

Significant group differences were noted in cecum histology (Figure 7A—D). In OM and OF mice, cecum crypts were 25—30% broader, visually disorganized, and reduced in number per slide compared to their LM and LF counterparts (Figure 7B,**C**). Additionally, crypt height was significantly reduced in OF mice compared to LF mice, a feature not observed in OM vs. LM comparisons (Figure 7D). Goblet cells, vital for synthesizing and secreting protective mucins, were significantly reduced in number and size by 25—30% in OM and OF mice compared to LM and LF, respectively (Figure 7B,C).

No differences in mRNA expression of gut permeability genes were detected between OM and LM mice (Figure 7E). Instead, gut permeability was significantly compromised in OF mice compared to LF mice, with measured markers showing reduced expression (Figure 7F). The observed damage to gut permeability was paralleled by reductions in the expression of mitochondrial biogenesis genes. In OF mice, mitochondrial gene expression was significantly impaired (Figure 7F), and PET imaging (Figure 7H) revealed increased glucose uptake in the cecum of OF mice compared to LF mice, whereas no such differences were noted between OM and LM groups (Figure 7E—G).

3.6. Metabolites suggest early functional conditioning of FMT linked to donor diet

Metabolomic analysis focused on metabolites with VIP scores >1 (Figure 8A—D) at 23 weeks revealed 19 and 6 discriminant fecal and plasma metabolites, respectively, in OF vs LF mice, and 21 and 12 metabolites in OM vs. LM mice. Post-hoc non-parametric group comparisons showed that OF (compared to LF) recipients exhibited significant deficits in fecal trimethylamine (TMA), trimethylamine-n-oxide (TMAO), and lysine, as well as in plasma TMA and 3-hydroxybutyrate (Figure 8E,F). Since lysine is crucial for ketogenesis, carnitine synthesis, and fatty acid oxidation, its reduction likely contributes to low plasma 3-hydroxybutyrate levels in OF mice, reflecting impaired liver ketogenesis and reduced lipid oxidation. These deficits cannot be attributed to differences in food intake, as all mice received the same diet, and OF mice consumed more food than LF mice. These results suggest insufficient metabolite production by the microbiota [45]. In contrast to OF recipients, OM mice showed an excess of the identified metabolites compared to LM mice, including fecal phenylalanine, glycine, alanine, xanthine, hypoxanthine, uracil, xylose, arabinose, formate, acetate, and lactate, and plasma lactate, citrate, and succinate (Figure 8G,I). High plasma levels of citrate, lactate, and succinate indicate impaired TCA cycle function [46], consistent with observed amino acid accumulation and whitening of BAT in OM mice. Importantly, OM mice consumed equal or less food than LM mice throughout the study, ruling out overeating as the cause for increased fecal metabolite levels. Notably, differences in fecal metabolite profiles observed at 23 weeks post-FMT were already evident at 1 or 15 weeks in both sexes (Figure 8J), suggesting a stable fecal metabolome over time (Fig. S3). To identify shared metabolites between donors and recipients, we compared metabolites in children with those in sex-matched mice at one week. Although NMR spectra

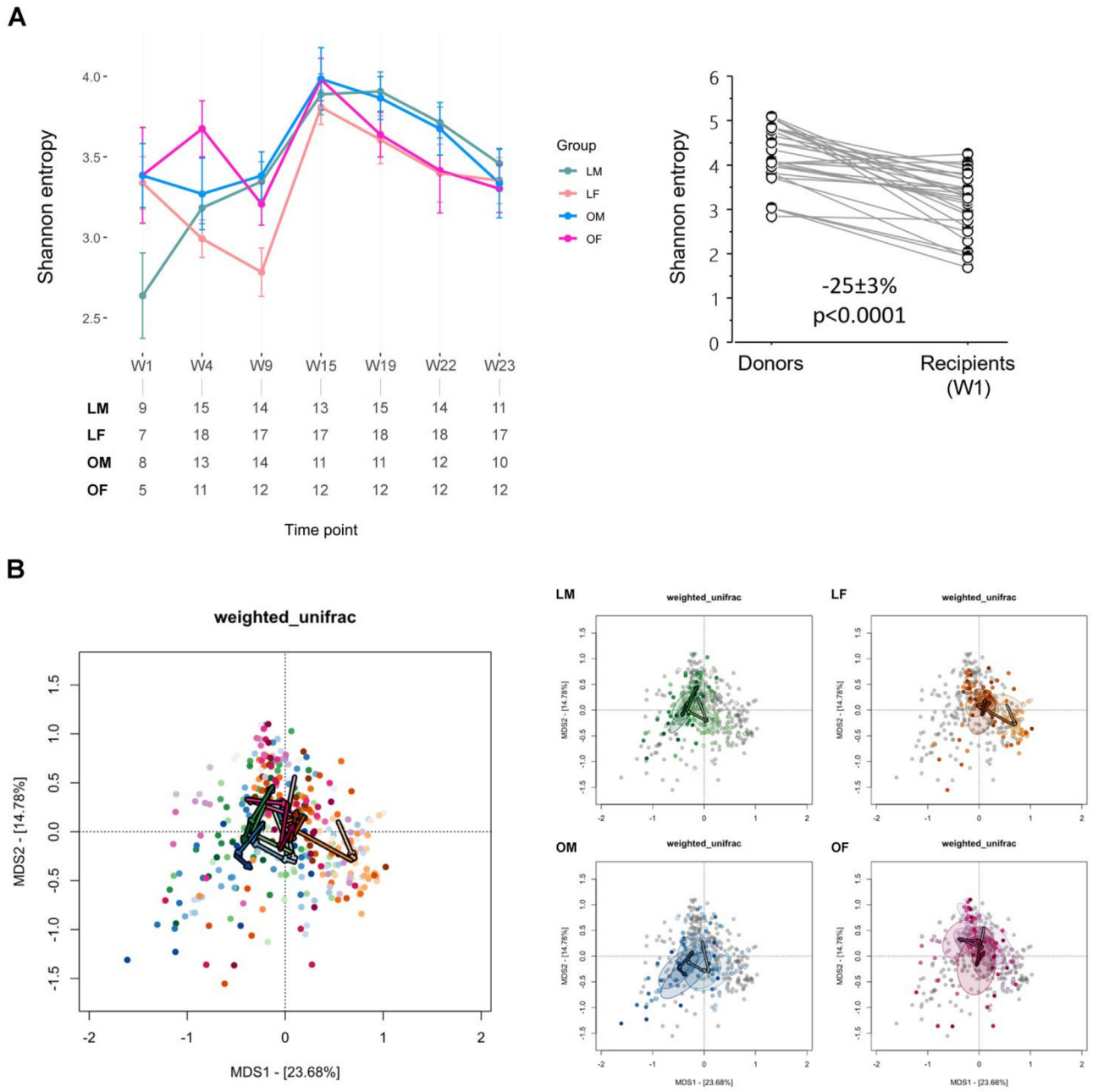

Figure 5: Temporal and phenotypic influences on microbial alpha and beta diversity following FMT in humanized mice. (A) On the left, longitudinal alpha diversity analysis conducted using Shannon entropy for the four groups of mice, labeled according to donor phenotype: lean female (LF), lean male (LM), obese female (OF), and obese male (OM). Alpha diversity analysis spans from the first week post-FMT (W1) to the final time point (week 23 = W23). On the right, paired t-test analysis of microbial biodiversity in children and their respective recipient mice. (B) Principal Coordinates Analysis (PCoA) based on weighted UniFrac distances among LM (green), LF (orange), OM (blue), and OF (pink) groups. Boxplots detailing the comparison between time points in each group are given in Fig. S2.

from children were less resolved, significant correlations emerged. For instance, fecal TMA levels correlated between girls and female mice, while fecal uracil, phenylalanine, glycine, and, to a lesser extent, alanine showed correlations between boys and male mouse recipients (Figure 8K). To generate mechanistic hypotheses, providing leads towards modifiable factors that may influence metabolite profiles, we then revisited the children's food frequency questionnaires completed at the time of fecal collection [19], addressing animal proteins (primary sources of amino acids, choline, carnitine, and TMA precursors), sugars and beverages (primary sources of acetate, lactate, xanthine, and hypoxanthine, e.g., from theophylline), dietary fibers (hemicellulose-derived sources of xylose and arabinose, which feed acetate and lipid formation) [47,48], and vegetables and fruits (sources of formate). Notably, female children with obesity had a lower percentage of caloric intake from animal proteins, whereas male children with obesity consumed higher amounts of animal proteins, simple sugars, and fibers. Male children with obesity also reported more frequent intake of vegetables, fruits, and packaged tea than other groups (Figure 8L,M). These findings underscore an early, potentially diet-mediated shaping of the gut ecosystem.

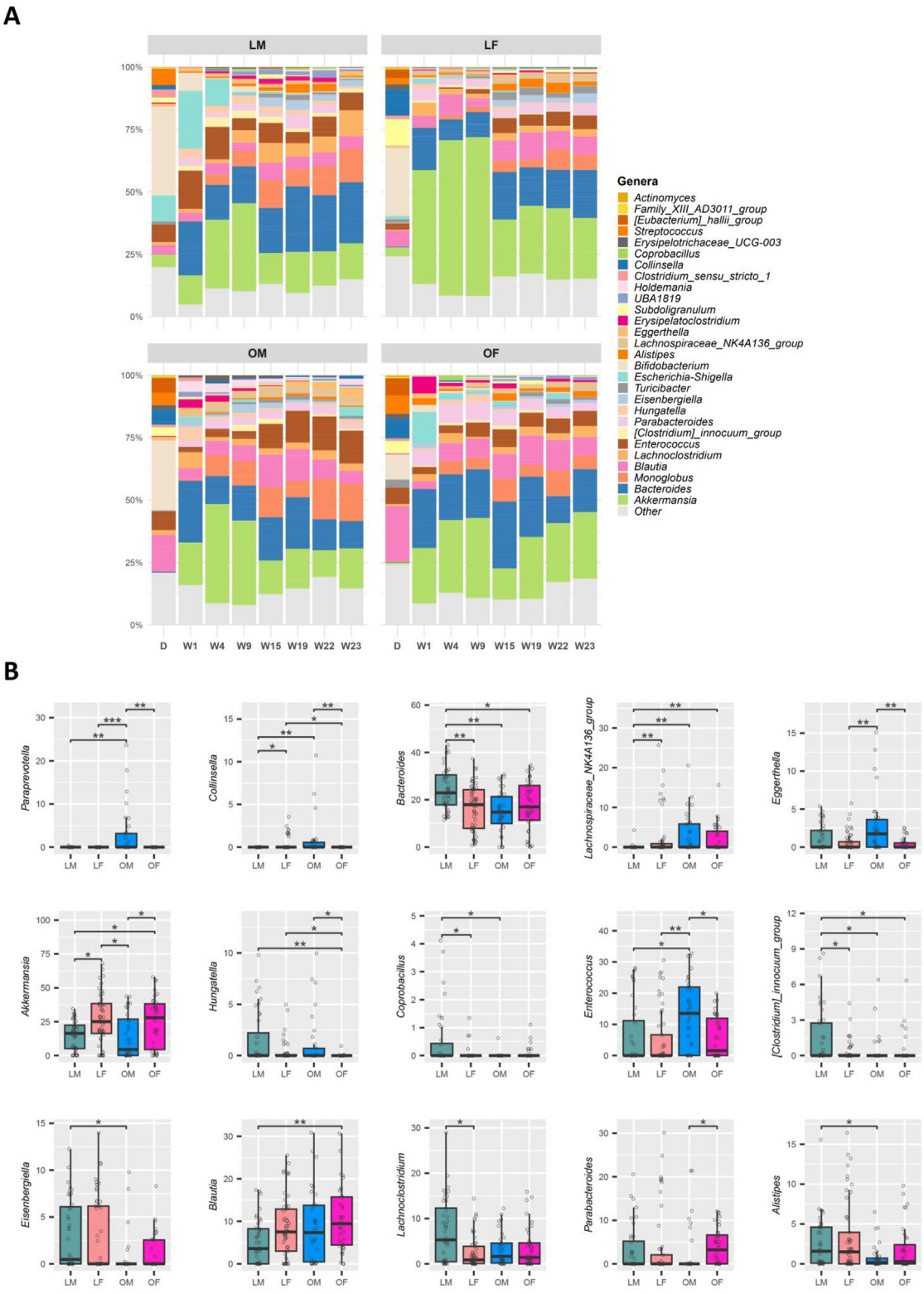

Figure 6: Temporal and phenotypic influences on microbial composition following FMT in humanized mice. (A) Bar plots showing the average relative abundance of gut microbiota genera groups over time from W1 (week one post-FMT) to W23 (week 23 post-FMT) including children donors' profiles (D), in mice recipient study groups named according to donors' phenotype: lean male (LM), lean female (LF), obese male (OM), and obese female (OF). Only bacterial genera with a relative abundance $\geq$0.2% in at least 1/6 of samples in each group are shown. (B) Boxplots showing the relative abundance distribution of bacterial genera significantly different between study groups: lean male (LM), lean female (LF), obese male (OM), and obese female (OF) recipient mice. In the boxplot, the compositional gut microbiota profiles were grouped at the timepoints W19, W22, and W23, to emphasize the differences following stabilization of the microbial ecosystem post-FMT. Sample size and distribution are shown by individual points in each boxplot. Wilcoxon test, FDR *, $p \leq 0.05$; **, $p \leq 0.01$; ***, $p \leq 0.001$.

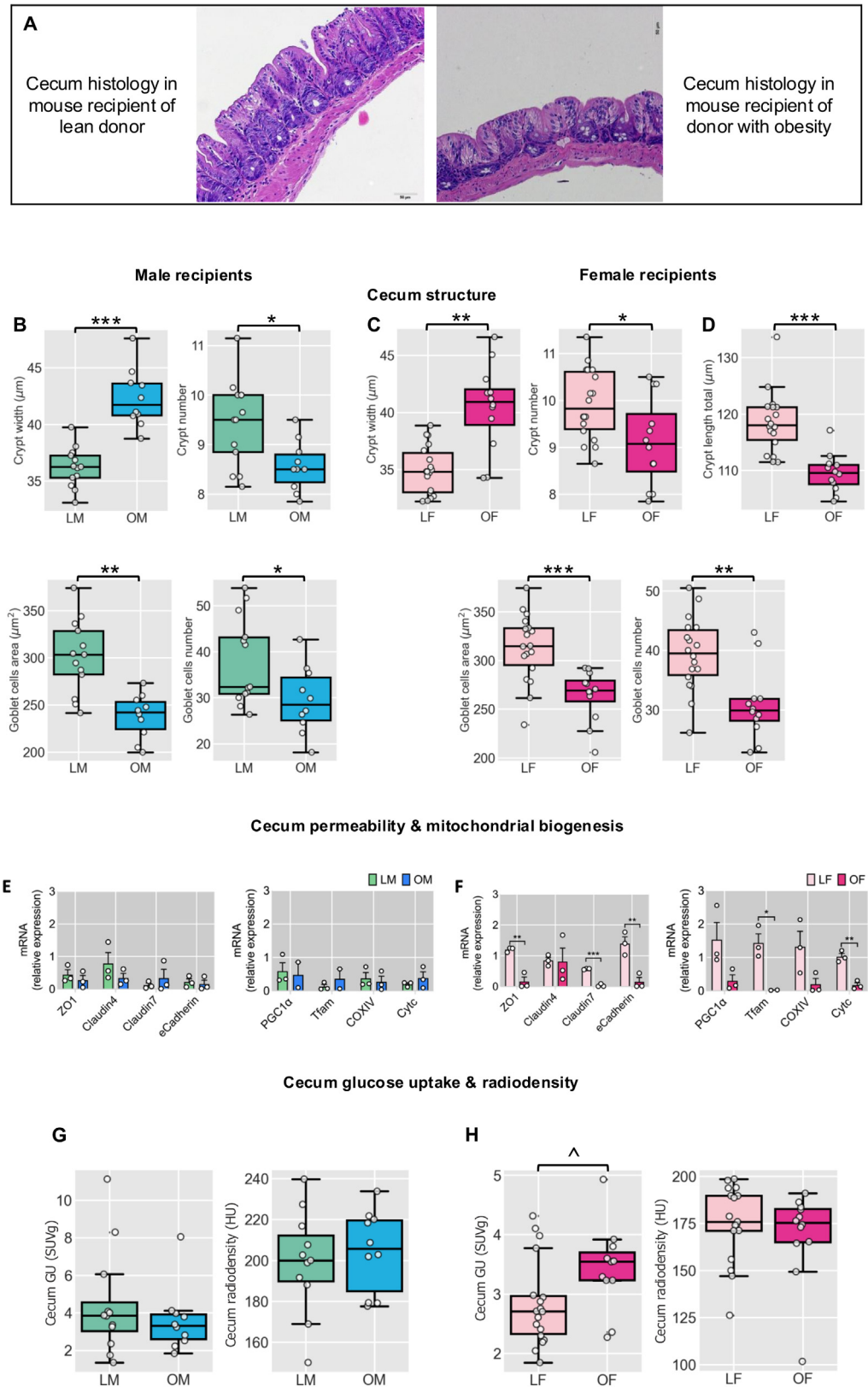

Figure 7: Gut histology, permeability, and mitochondrial biogenesis in FMT mice recipients. (A) Representative example of histological cecum slides for each group. (B—D) Group averages of histological gut parameters in male (B) and female (C—D) mice recipients of lean (LM, LF) or obese donors (OM, OF). (E—F) Tissue mRNA expression of markers of cecum permeability and mitochondrial activity in male (E) and female (F) mice. (G—H) PET and CT-derived glucose uptake and radiodensity in the cecum *in vivo*. Sample size and distribution are shown by individual points in each box-plot. *$p < 0.05$; **$p < 0.01$; ***$p < 0.0001$; ^$p < 0.059$. Recipient groups are labeled according to donor phenotype: lean male (LM), lean female (LF), obese male (OM), and obese female (OF).

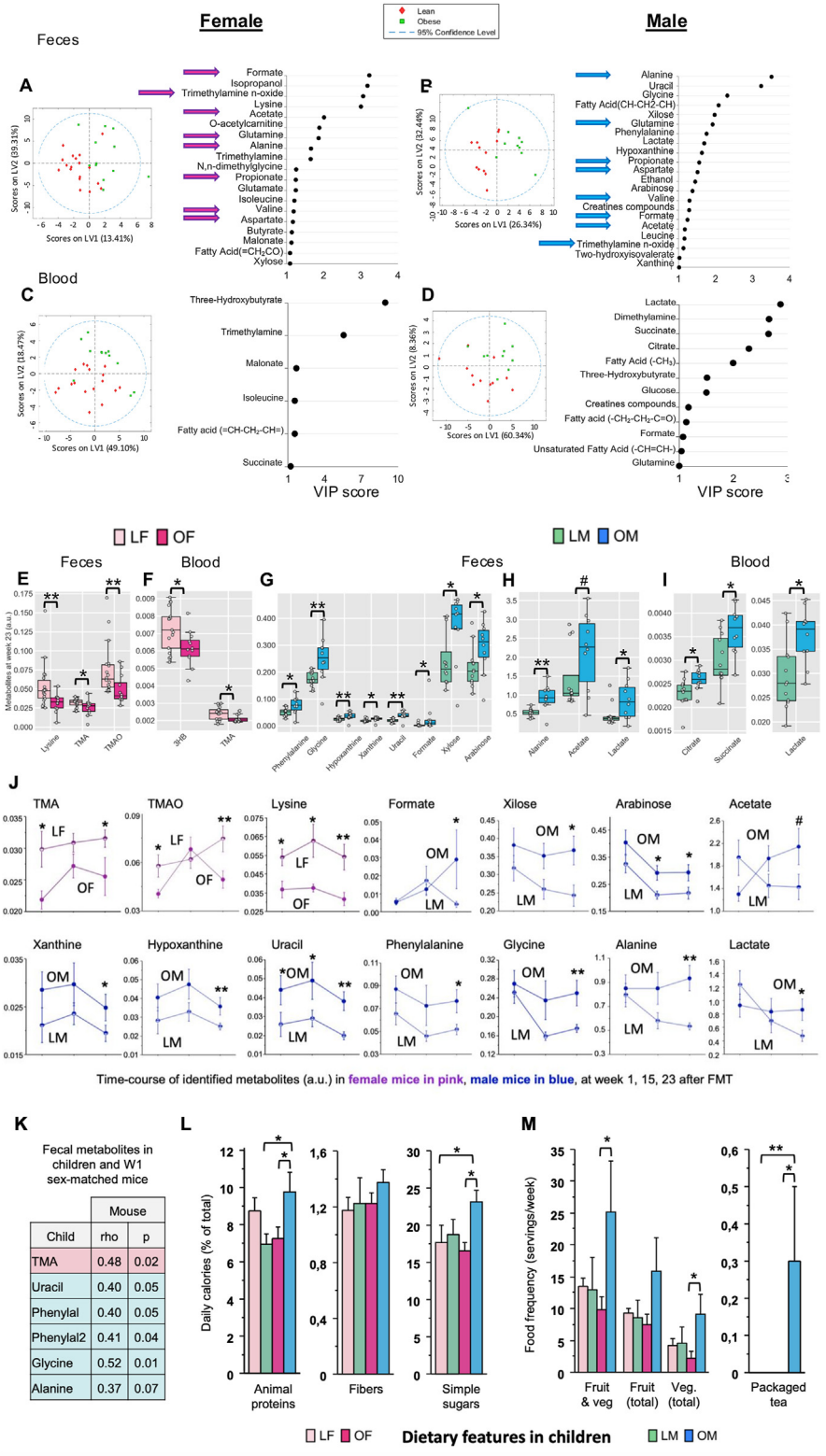

	Mouse	
Child	rho	p
TMA	0.48	0.02
Uracil	0.40	0.05
Phenylal	0.40	0.05
Phenylal2	0.41	0.04
Glycine	0.52	0.01
Alanine	0.37	0.07

Figure 8: Fecal and plasma metabolites suggest early functional conditioning of FMT microbiota linked to donor diet. (A—D) Metabolites were measured by NMR spectroscopy and examined by PLS-DA followed by Variable Importance in Projection (VIP) scores analysis in feces (A—B) and blood (C—D) in female (A, C) and male mice (B, D), labeled according to their FMT donor phenotype: lean male (LM), lean female (LF), obese male (OM), and obese female (OF). An overview of all metabolites at three time points (week 1, week 15, week 23 post-FMT) is shown in Fig. S3. (E—H). Non-parametric comparisons between mouse groups (23 weeks) were used to select the most significant metabolites (E—I); boxplots show samples and distributions by individual points. (J—K) The emerging fecal metabolites of mice were observed over time, namely at 1, 15, 23 weeks post-FMT (J), and their levels at 1 week post-FMT showed correlations (Spearman) (K) against sex-matched child donors. (L, M) Child intakes of main dietary sources of metabolites by analysis of variance of validated questionnaire data and calculations based on reference databases (as explained in text). *$p < 0.05$; **$p < 0.01$, #$p = 0.11$.

3.7. Multi-omics integration analysis

We performed a comprehensive multi-omics integration analysis to correlate gut microbiota composition at 23 weeks with morphological, metabolomic, and body parameters in mice. N-integration analysis revealed strong correlations ($r > 0.7$, $p < 0.05$) involving *Collinsella* and *Eggertella* genera with multiple biochemical, morphological, and physiological parameters (Figs. S4 and S5; Table S5). Both genera were relatively less abundant in female mice and highly abundant in OM mice. Notably, *Eggertella* abundance showed positive correlations with body weight, BAT and PVAT expansion, and $scWAT_i$ whitening, which were all more pronounced in OM recipients. Additionally, *Eggertella* was associated with saturated fatty acids and dimethylamine levels, identified as key metabolites in male mice based on VIP scores. Meanwhile, *Collinsella* abundance was associated with lower fecal lysine abundance in OF mice, aligning with observed deficits in ketogenesis and lipid oxidation.

4. DISCUSSION

This study demonstrates that a single early-life FMT from young children, either with or without obesity, induces significant and long-lasting effects on the maturation of intestinal and adipose tissues in mice, persisting into adulthood. This finding underscores the critical influence of early microbiota composition on long-term metabolic and tissue development. The study was conducted in sex-matched donors and recipients. Male recipients exhibited extensive adipose tissue whitening, a hallmark often associated with reduced thermogenic capacity and metabolic dysfunction. In contrast, female recipients showed a distinct profile characterized by enhanced diabetogenic and inflammatory traits.

The primary impact of FMT was observed on gut barrier function, a critical determinant of systemic metabolic health. A healthy gut barrier relies on high cellular turnover, selective permeability, and efficient energy provision, which in turn depends on mitochondrial function and structural integrity supported by cellular reservoirs, the mucus layer, and junction-anchoring proteins. In female mice receiving FMT from girls with obesity, these features were severely compromised, promoting chronic inflammation of the gut wall and scWAT that persisted into adulthood. These female recipient mice consumed more food but exhibited impaired $scWAT_i$ expandability and lacked the typical whitening of BAT. Fat accumulation was instead restricted to visceral adipose depots, a phenotype associated with metabolic dysregulation. Conversely, male mice receiving FMT from boys with obesity showed diffuse lipid storage across adipose depots and significant accumulation of BCAA and other amino acids in BAT, consistent with a high clearance rate of these metabolites [49]. Notably, while BCAA levels were high in both feces (VIP score$>$1) and BAT in OM mice, they did not differ in LM and OM mice groups in the circulation, suggesting efficient metabolic processing within BAT. Additional amino acids, including alanine, phenylalanine, and glycine, were elevated in both feces and BAT in males receiving FMT from boys with obesity (OM group). These observations align with the known role of BCAA-derived metabolites in promoting lipid droplet formation in adipocytes, enhancing glucose transport, and stimulating *de novo* lipogenesis in BAT [41]. The metabolic profile of OM mice, characterized by high glucose uptake and lipid droplet formation across all adipose depots, was accompanied by an increase in circulating intermediates of the TCA cycle — namely citrate, succinate, and lactate. This suggests a downregulation of substrate catabolism, further supporting the distinct metabolic adaptations induced by FMT. Female mice typically exhibit more active BAT, potentially due to more efficient mitochondrial function, which is in line with our results [50]. Interestingly, the sex-dimorphic mice phenotypes observed in WAT, BAT, obesity, glycemia in this study are strikingly similar to those reported in mice offsprings exposed to a high-fat diet during gestation and lactation through their dams [8]. In such models, specific gut microbiota signatures have been suggested as being implicated in programming these phenotypes, underscoring the potential role of the microbiota in shaping long-term metabolic outcomes. Although sex-specific microbiome signatures have been implicated in differential susceptibility to obesity and metabolic disorders [51,52], our use of sex-matched donors and recipients limits the ability to disentangle the independent effects of sex from those of fecal microbiota composition.

The genus *Collinsella*, emerging in this study, displayed higher abundance in OM mice and lower abundance in OF mice compared to their respective controls. *Collinsella* is known to produce TMA and acetate [53] and possesses protective properties by breaking down fructose-lysine [54]. These properties align well with the observed fecal metabolic profiles: high acetate levels in OM and low TMA and lysine levels in OF. Additionally, *Collinsella* abundance was strongly correlated with fecal lysine abundance in DIABLO analysis. The high fecal lactate levels in OM mice may be attributed to the abundance of *Enterococcus*, a lactate-producing genus. Furthermore, *Lachnospiraceae NK4A136*, known for its probiotic properties, and *Paraprevotella*, a succinate producer involved in BCAA metabolism, may contribute to the less aggressive metabolic phenotype observed in male mice compared to females receiving FMT from children with obesity. Overall, the microbiota profile in OM recipients—characterized by high abundance of *Paraprevotella*, *Collinsella*, *Lachnospiraceae NK4A136*, along with low abundance of *Bacteroides* and *Coprobacillus* [55]—is typically associated with an improved lipid profile, reduced inflammation, and enhanced insulin sensitivity. These outcomes have been demonstrated in various metabolic interventions, including dietary changes, prebiotics, probiotics, symbiotics, FMT, and physical activity, as recently reviewed [56].

Functional redundancy of the gut microbiota is a well-known phenomenon [57], and this study provides first demonstration that the microbiota of children, when transplanted into young, sex-matched mice, retains its initial metabolic functionality into adulthood. This occurs despite the transplantation being performed only once and subsequent shifts in bacterial composition driven by the host environment, diet, and physical growth. Remarkably, most identified metabolites exhibited significant alterations shortly after FMT and maintained these altered states through adulthood. Furthermore, several metabolite levels in the mice correlated with fecal metabolite levels in the corresponding child donors, conferring translational value to these results.

In addition, we observed that dietary patterns in child donors were consistent with profiles in feces of recipient mice, generating the hypothesis that early-life dietary impacts on microbiota function can persist into adulthood, even after a prolonged period of dietary standardization following FMT, which merits proof-of-concept demonstration.

For example, consumption of animal-derived food products, which promotes the enrichment of the *Collinsella* genus and provides a primary source of amino acids and TMA precursors, was lower in female children with obesity, whereas male children with obesity consumed these products in higher amounts. Additionally, high intake of simple sugars among male child donors was associated with an abundance of fecal glycolytic bacteria and metabolites in recipient mice. Notably, these children also consumed more dietary

fiber, in line with elevated fecal arabinose and xylose levels in male mice recipients, while their high theophylline intake corresponded with increased fecal xanthine levels. These findings potentially entail relevant implications, since the significant and lasting opportunity for an early-life diet to shape the microbiota, effectively creating a form of ecosystem with enduring consequences could represent a robust strategy for primary prevention.

The strengths and novelties of this study are manifolds. First, to our knowledge, it is the first study of this kind with a prolonged follow-up period post-FMT. A 5-month lifespan in mice corresponds to approximately 20–30 years in humans, making this a meaningful model for long-term microbiota–host interactions. The use of single FMT, rather than multiple treatments, was crucial to testing the hypothesis that early-life microbiota imprinting programs health outcomes in adulthood—a key finding with significant clinical implications. Second, we uncovered sex-dimorphic outcomes of early-life FMT from children with obesity, with male mice recipients exhibiting a greater propensity for obesity, whereas female mice showed a higher risk for diabetes-like traits. Third, the incorporation of imaging techniques in this study provided organ-specific, *in vivo* insights into cause–effect relationships, significantly enhancing the translational relevance of our findings. Finally, we identified mechanistic leads, including fecal metabolite signatures and BAT BCAA dynamics, which combined with the emerging hypothesis on diet–microbiota interactions, offer preventive perspectives on early-dietary interventions.

Our study has several limitations. While animal models enable the investigation of potential mechanisms that are not feasible in humans, they remain approximations of complex human physiology. In our case, demonstrating causal relationships in humans would require decades of follow-up, during which numerous confounding factors could arise. Moreover, direct access to relevant tissue is not possible in longitudinal human studies, further limiting mechanistic insights. While we acknowledge that transferring microbiota between species can introduce artifacts, our results nonetheless provide significant proof of principle that compositional differences in fecal matter can influence AT development, as evidenced by shared phenotypes and metabolites between donors and recipients. Another limitation lies in the varying quality of metabolite spectra resolution between human and mouse feces, which may affect the precision of metabolic comparisons. Additionally, although sex-matching donor–recipient pairs was essential for maintaining physiological consistency, future studies using sex-discordant pairs may help disentangle the specific contributions of sex to the sex-dimorphic outcomes observed. However, such designs may introduce hormonal and physiological mismatches, potentially confounding - or even opposing - the isolated effects of FMT [58,59]. Moreover, other tissues like liver and pancreas play an important role in the development of obesity and associated metabolic diseases, and will be future targets, as we investigate their role in relation to FMT and the current findings. Lastly, targeted experiments are needed to confirm whether individual dietary components can induce lasting changes in microbiota function, even after their removal, which has important implications for data interpretation in the field.

In conclusion, our findings contribute significantly to demonstrate the lasting impact of early-life timing on the fecal microbiological and metabolic environment. This metabolic imprint is stably transferred via FMT, persisting from infancy to adulthood in recipients and shaping the development of adipose tissue, intestinal structure, and glucose homeostasis. Dietary habits in human donors were coherent with fecal metabolic profiles observed in their corresponding adult mice recipients. Although findings from animal studies are not directly translatable to humans, the persistence of these fecal signatures - despite changes in the host, environment, and diet - highlights the need to identify and optimize beneficial exposures during early life.

ACKNOWLEDGMENTS

We are grateful to the Animal Care staff for their constant and expert support. This study was conducted within the JPIHDHL-INTIMIC Joint Transnational Research program (project no. INTIMIC-085 GUTMOM, Italian Ministry of University and Research, Ministry Decree no. 946/2019) to PI (Consortium coordinator) and to DM (Partner), and the JPI-HDHL-INTIMIC Knowledge Platform of Food, Diet, Intestinal Microbiomics, and Human Health (sub-project no. KP-778 MISVILUPPO, Italian Ministry of Agricultural, Food and Forestry Policies, Ministry Decree 23092/7303/19) to PI (Partner).

This work was also supported by grants from EFSD/Boehringer Ingelheim European Research Programme on "Multi-System Challenges of Diabetes" 2023 to PI; CNR project FOE-2021 DBA.AD005.225 to MAG; Progetti di Ricerca di Rilevante Interesse Nazionale (Prin) Bando 2020 [Prot. 20205X4C9E] and Bando 2022 [Prot. 2022XZ7MBC] to EN; Professional Dietetics S.p.A. (Milan, Italy) to EN; SOE_0000181 [MUR Concession Decree no. 564 of 13/12/2022, CUP C93C22007650006, funded under the National Recovery and Resilience Plan (NRRP), Mission 4, Component 2, Investment 1.2, MUR Call for tender n. 367 of 7/10/2022 funded by the European Union – NextGenerationEU] to CR.

DM gratefully acknowledges funding from grants PID2019-108973RB-C22 and PCIN2017-117 from the Ministerio de Ciencia e Innovación of Spain, and GV/2020/048, IDIFEDER/2021/072 and CIAICO/2022/181 from the Generalitat Valenciana of Spain.

MPT was supported by the Ministry of University of Spain and the University of Valencia, by Next Generation EU funds (MS21-086).

The funders had no role in study design, data collection and analysis, or preparation of the manuscript.

CRediT AUTHORSHIP CONTRIBUTION STATEMENT

Federica La Rosa: Writing – review & editing, Investigation, Formal analysis, Data curation. **Maria Angela Guzzardi:** Writing – review & editing, Supervision, Investigation, Formal analysis, Data curation, Conceptualization. **Mercedes Pardo-Tendero:** Methodology, Formal analysis. **Monica Barone:** Writing – review & editing, Methodology, Formal analysis. **Chiara Ruocco:** Writing – review & editing, Methodology, Formal analysis. **Gabriele Conti:** Methodology, Formal analysis. **Daniele Panetta:** Methodology, Investigation. **Daria Riabitch:** Methodology, Formal analysis. **Silvia Bernardi:** Formal analysis. **Assuero Giorgetti:** Methodology. **Daniela Campani:** Methodology. **Daniel Monleon:** Methodology, Funding acquisition, Formal analysis. **Enzo Nisoli:** Writing – review & editing, Methodology, Funding acquisition, Formal analysis. **Patrizia Brigidi:** Writing – review & editing, Methodology, Formal analysis. **Patricia Iozzo:** Writing – review & editing, Writing – original draft, Supervision, Funding acquisition, Formal analysis, Conceptualization.

DECLARATION OF COMPETING INTEREST

The authors declare that they have no known competing financial interests or personal relationships that could have appeared to influence the work reported in this paper.

DATA AVAILABILITY

Data will be made available on request.

APPENDIX A. SUPPLEMENTARY DATA

Supplementary data to this article can be found online at https://doi.org/10.1016/j.molmet.2025.102157.

REFERENCES

[1] Hannon TS, Arslanian SA. Obesity in adolescents. N Engl J Med 2023;389:251–61. https://doi.org/10.1056/NEJMcp2102062.

[2] Twig G, Yaniv G, Levine H, Leiba A, Goldberger N, Derazne E, et al. Body-mass index in 2.3 million adolescents and cardiovascular death in adulthood. N Engl J Med 2016;374:2430–40. https://doi.org/10.1056/NEJMoa1503840.

[3] Lindberg L, Danielsson P, Persson M, Marcus C, Hagman E. Association of childhood obesity with risk of early all-cause and cause-specific mortality: a Swedish prospective cohort study. PLoS Med 2020;17:e1003078. https://doi.org/10.1371/journal.pmed.1003078.

[4] Anekwe CV, Jarrell AR, Townsend MJ, Gaudier GI, Hiserodt JM, Stanford FC. Socioeconomics of obesity. Curr Obes Rep 2020;9:272–9. https://doi.org/10.1007/s13679-020-00398-7.

[5] Reinehr T. Type 2 diabetes mellitus in children and adolescents. World J Diabetes 2013;4:270–81. https://doi.org/10.4239/wjd.v4.i6.270.

[6] Hillier TA, Pedula KL. Complications in young adults with early-onset type 2 diabetes: losing the relative protection of youth. Diabetes Care 2003;26:2999–3005. https://doi.org/10.2337/diacare.26.11.2999.

[7] Huang RC, Mori TA, Burrows S, Le Ha C, Oddy WH, Herbison C, et al. Sex dimorphism in the relation between early adiposity and cardiometabolic risk in adolescents. J Clin Endocrinol Metab 2012;97:E1014–22. https://doi.org/10.1210/jc.2011-3007.

[8] Guzzardi MA, Collado MC, Panetta D, Tripodi M, Iozzo P. Maternal high-fat diet programs white and brown adipose tissues in vivo in mice, with different metabolic and microbiota patterns in obesity-susceptible or obesity-resistant offspring. Metabolites 2022;12. https://doi.org/10.3390/metabo12090828.

[9] Guzzardi MA, La Rosa F, Campani D, Cacciato Insilla A, De Sena V, Panetta D, et al. Maturation of the visceral (Gut-Adipose-Liver) network in response to the weaning reaction versus adult age and impact of maternal high-fat diet. Nutrients 2021;13. https://doi.org/10.3390/nu13103438.

[10] Dalby MJ. Questioning the foundations of the gut microbiota and obesity. Philos Trans R Soc Lond B Biol Sci 2023;378:20220221. https://doi.org/10.1098/rstb.2022.0221.

[11] Li M, Li L, Li B, Hambly C, Wang G, Wu Y, et al. Brown adipose tissue is the key depot for glucose clearance in microbiota depleted mice. Nat Commun 2021;12:4725. https://doi.org/10.1038/s41467-021-24659-8.

[12] Bifari F, Ruocco C, Decimo I, Fumagalli G, Valerio A, Nisoli E. Amino acid supplements and metabolic health: a potential interplay between intestinal microbiota and systems control. Gene Nutr 2017;12:27. https://doi.org/10.1186/s12263-017-0582-2.

[13] Guzzardi MA, La Rosa F, Iozzo P. Trust the gut: outcomes of gut microbiota transplant in metabolic and cognitive disorders. Neurosci Biobehav Rev 2023;149:105143. https://doi.org/10.1016/j.neubiorev.2023.105143.

[14] Suarez-Zamorano N, Fabbiano S, Chevalier C, Stojanovic O, Colin DJ, Stevanovic A, et al. Microbiota depletion promotes browning of white adipose tissue and reduces obesity. Nat Med 2015;21:1497–501. https://doi.org/10.1038/nm.3994.

[15] Han HS, Ahn E, Park ES, Huh T, Choi S, Kwon Y, et al. Impaired BCAA catabolism in adipose tissues promotes age-associated metabolic derangement. Nat Aging 2023;3:982–1000. https://doi.org/10.1038/s43587-023-00460-8.

[16] Yoshida N, Yamashita T, Osone T, Hosooka T, Shinohara M, Kitahama S, et al. Bacteroides spp. promotes branched-chain amino acid catabolism in brown fat and inhibits obesity. iScience 2021;24:103342. https://doi.org/10.1016/j.isci.2021.103342.

[17] Guzzardi MA, La Rosa F, Granziera F, Panetta D, Pardo-Tendero M, Barone M, et al. Gut-derived metabolites mediating cognitive development in 5-year-old children: early-life transplant in mice has lasting effects throughout adulthood. Brain Behav Immun 2023;114:94–110. https://doi.org/10.1016/j.bbi.2023.08.009.

[18] Guzzardi MA, Granziera F, Sanguinetti E, Ditaranto F, Muratori F, Iozzo P. Exclusive breastfeeding predicts higher hearing-language development in girls of preschool age. Nutrients 2020;12. https://doi.org/10.3390/nu12082320.

[19] Granziera F, Guzzardi MA, Iozzo P. Associations between the Mediterranean diet pattern and weight status and cognitive development in preschool children. Nutrients 2021;13. https://doi.org/10.3390/nu13113723.

[20] Censi L, D'Addesa D, Galeone D, Andreozzi S, Spinelli A. Studio ZOOM8 : l'alimentazione e l'attività fisica dei bambini della scuola primaria (Roma : Istituto Superiore di Sanità. 2012.

[21] Food composition database for epidemiological studies in Italy (BDA) (in Italian). https://bda.ieo.it/?page_id=690&lang=en.

[22] Council for Agricultural Research and Agricultural economics analysis (CREA) (in Italian). https://www.crea.gov.it/-/tabella-di-composizione-degli-alimenti.

[23] Guidelines for a healthy diet. Scientific Dossier 2018 [Chapter 10, pages 1123-1235] (in Italian), https://www.crea.gov.it/web/alimenti-e-nutrizione/-/dossier-scientifico-linee-guida-per-una-sana-alimentazione-2018.

[24] Hong SJ, Lee JH, Kim EJ, Yang HJ, Park JS, Hong SK. Anti-obesity and anti-diabetic effect of neoagarooligosaccharides on high-fat diet-induced obesity in mice. Mar Drugs 2017;15. https://doi.org/10.3390/md15040090.

[25] Thompson HJ, McGinley JN, Neil ES, Brick MA. Beneficial effects of common bean on adiposity and lipid metabolism. Nutrients 2017;9. https://doi.org/10.3390/nu9090998.

[26] Zarrinpar A, Chaix A, Xu ZZ, Chang MW, Marotz CA, Saghatelian A, et al. Antibiotic-induced microbiome depletion alters metabolic homeostasis by affecting gut signaling and colonic metabolism. Nat Commun 2018;9:2872. https://doi.org/10.1038/s41467-018-05336-9.

[27] Ragni M, Ruocco C, Tedesco L, Carruba MO, Valerio A, Nisoli E. An amino acid-defined diet impairs tumour growth in mice by promoting endoplasmic reticulum stress and mTOR inhibition. Mol Metabol 2022;60:101478. https://doi.org/10.1016/j.molmet.2022.101478.

[28] Ruocco C, Ragni M, Tedesco L, Segala A, Servili M, Riccardi G, et al. Molecular and metabolic effects of extra-virgin olive oil on the cardiovascular gene signature in rodents. Nutr Metabol Cardiovasc Dis 2022;32:1571–82. https://doi.org/10.1016/j.numecd.2022.03.020.

[29] Lee B, Moon KM, Kim CY. Tight junction in the intestinal epithelium: its association with diseases and regulation by phytochemicals. J Immunol Res 2018;2018:2645465. https://doi.org/10.1155/2018/2645465.

[30] Guerbette T, Boudry G, Lan A. Mitochondrial function in intestinal epithelium homeostasis and modulation in diet-induced obesity. Mol Metabol 2022;63:101546. https://doi.org/10.1016/j.molmet.2022.101546.

[31] Barone M, Garelli S, Rampelli S, Agostini A, Matysik S, D'Amico F, et al. Multi-omics gut microbiome signatures in obese women: role of diet and uncontrolled eating behavior. BMC Med 2022;20:500. https://doi.org/10.1186/s12916-022-02689-3.

[32] Masella AP, Bartram AK, Truszkowski JM, Brown DG, Neufeld JD. PANDAseq: paired-end assembler for illumina sequences. BMC Bioinf 2012;13:31. https://doi.org/10.1186/1471-2105-13-31.

[33] Bolyen E, Rideout JR, Dillon MR, Bokulich NA, Abnet CC, Al-Ghalith GA, et al. Reproducible, interactive, scalable and extensible microbiome data science using QIIME 2. Nat Biotechnol 2019;37:852–7. https://doi.org/10.1038/s41587-019-0209-9.

[34] Callahan BJ, McMurdie PJ, Rosen MJ, Han AW, Johnson AJ, Holmes SP. DADA2: high-resolution sample inference from Illumina amplicon data. Nat Methods 2016;13:581–3. https://doi.org/10.1038/nmeth.3869.

[35] Quast C, Pruesse E, Yilmaz P, Gerken J, Schweer T, Yarza P, et al. The SILVA ribosomal RNA gene database project: improved data processing and web-based tools. Nucleic Acids Res 2013;41:D590–6. https://doi.org/10.1093/nar/gks1219.

[36] Edgar RC. Search and clustering orders of magnitude faster than BLAST. Bioinformatics 2010;26:2460–1. https://doi.org/10.1093/bioinformatics/btq461.

[37] Robeson MS, O'Rourke 2nd DR, Kaehler BD, Ziemski M, Dillon MR, Foster JT, et al. RESCRIPt: reproducible sequence taxonomy reference database management. PLoS Comput Biol 2021;17:e1009581. https://doi.org/10.1371/journal.pcbi.1009581.

[38] Bokulich NA, Kaehler BD, Rideout JR, Dillon M, Bolyen E, Knight R, et al. Optimizing taxonomic classification of marker-gene amplicon sequences with QIIME 2's q2-feature-classifier plugin. Microbiome 2018;6:90. https://doi.org/10.1186/s40168-018-0470-z.

[39] FabbriniMarco/microbAIDeR. An ensemble of functions for easier and quicker preliminary microbiome analyses. 2023. https://github.com/FabbriniMarco/microbAIDeR.

[40] Le Cao KA, Costello ME, Lakis VA, Bartolo F, Chua XY, Brazeilles R, et al. MixMC: a multivariate statistical framework to gain insight into microbial communities. PLoS One 2016;11:e0160169. https://doi.org/10.1371/journal.pone.0160169.

[41] Wang Z, Wang QA, Liu Y, Jiang L. Energy metabolism in brown adipose tissue. FEBS J 2021;288:3647–62. https://doi.org/10.1111/febs.16015.

[42] Singh P, Gollapalli K, Mangiola S, Schranner D, Yusuf MA, Chamoli M, et al. Taurine deficiency as a driver of aging. Science 2023;380:eabn9257. https://doi.org/10.1126/science.abn9257.

[43] Sharon G, Cruz NJ, Kang DW, Gandal MJ, Wang B, Kim YM, et al. Human gut microbiota from autism spectrum disorder promote behavioral symptoms in mice. Cell 2019;177:1600–18. https://doi.org/10.1016/j.cell.2019.05.004.

[44] Staley C, Kaiser T, Beura LK, Hamilton MJ, Weingarden AR, Bobr A, et al. Stable engraftment of human microbiota into mice with a single oral gavage following antibiotic conditioning. Microbiome 2017;5:87. https://doi.org/10.1186/s40168-017-0306-2.

[45] Metges CC, Eberhard M, Petzke KJ. Synthesis and absorption of intestinal microbial lysine in humans and non-ruminant animals and impact on human estimated average requirement of dietary lysine. Curr Opin Clin Nutr Metab Care 2006;9:37–41. https://doi.org/10.1097/01.mco.0000196142.72985.d3.

[46] Fernandez-Veledo S, Marsal-Beltran A, Vendrell J. Type 2 diabetes and succinate: unmasking an age-old molecule. Diabetologia 2024;67:430–42. https://doi.org/10.1007/s00125-023-06063-7.

[47] Tomioka S, Seki N, Sugiura Y, Akiyama M, Uchiyama J, Yamaguchi G, et al. Cooperative action of gut-microbiota-accessible carbohydrates improves host metabolic function. Cell Rep 2022;40:111087. https://doi.org/10.1016/j.celrep.2022.111087.

[48] Takeuchi T, Kubota T, Nakanishi Y, Tsugawa H, Suda W, Kwon AT, et al. Gut microbial carbohydrate metabolism contributes to insulin resistance. Nature 2023;621:389–95. https://doi.org/10.1038/s41586-023-06466-x.

[49] Brown Z, Yoneshiro T. Brown fat thermogenesis and branched-chain amino acids in metabolic disease. Endocr J 2024;71:89–100. https://doi.org/10.1507/endocrj.EJ23-0205.

[50] Ventura-Clapier R, Moulin M, Piquereau J, Lemaire C, Mericskay M, Veksler V, et al. Mitochondria: a central target for sex differences in pathologies. Clin Sci (Lond) 2017;131:803–22. https://doi.org/10.1042/CS20160485.

[51] Min Y, Ma X, Sankaran K, Ru Y, Chen L, Baiocchi M, et al. Sex-specific association between gut microbiome and fat distribution. Nat Commun 2019;10:2408. https://doi.org/10.1038/s41467-019-10440-5.

[52] Peng C, Xu X, Li Y, Li X, Yang X, Chen H, et al. Sex-specific association between the gut microbiome and high-fat diet-induced metabolic disorders in mice. Biol Sex Differ 2020;11(5). https://doi.org/10.1186/s13293-020-0281-3.

[53] Liu Y, Dai M. Trimethylamine N-Oxide generated by the gut microbiota is associated with vascular inflammation: new insights into atherosclerosis. Mediat Inflamm 2020;2020:4634172. https://doi.org/10.1155/2020/4634172.

[54] Wolf AR, Wesener DA, Cheng J, Houston-Ludlam AN, Beller ZW, Hibberd MC, et al. Bioremediation of a common product of food processing by a human gut bacterium. Cell Host Microbe 2019;26:463–477 e468. https://doi.org/10.1016/j.chom.2019.09.001.

[55] Torres-Sanchez A, Ruiz-Rodriguez A, Ortiz P, Aguilera M. Key stratification of microbiota taxa and metabolites in the host metabolic health-disease balance. Int J Mol Sci 2023;24. https://doi.org/10.3390/ijms24054519.

[56] Tassoni DS, Macedo RCO, Delpino FM, Santos HO. Gut microbiota and obesity: the chicken or the egg? Obesities 2023;3:296–321. https://doi.org/10.3390/obesities3040024.

[57] Moya A, Ferrer M. Functional redundancy-induced stability of gut microbiota subjected to disturbance. Trends Microbiol 2016;24:402–13. https://doi.org/10.1016/j.tim.2016.02.002.

[58] Benedek G, Zhang J, Nguyen H, Kent G, Seifert HA, Davin S, et al. Estrogen protection against EAE modulates the microbiota and mucosal-associated regulatory cells. J Neuroimmunol 2017;310:51–9. https://doi.org/10.1016/j.jneuroim.2017.06.007.

[59] Org E, Mehrabian M, Parks BW, Shipkova P, Liu X, Drake TA, et al. Sex differences and hormonal effects on gut microbiota composition in mice. Gut Microbes 2016;7:313–22. https://doi.org/10.1080/19490976.2016.1203502.

